High Frequency Wave Propagation: a Convergent Approach, Part II: Implementation and Numerical Testing

Khoa D. Tran
Departments of Mathematics and Computer Science
University of Texas at Austin
khoa@math.utexas.edu
http://www.khoatran.com

December 7, 2005

Abstract

Numerical approximation of wave propagation is prevalent in many applications. When the wave frequency is high, this is a computationally challenging problem and is a study of interest. In this paper, I present the implementation and numerical testing of the convergent approach proposed by Bruno et al. and retheorized by Tran to solve problems of electromagnetic or acoustic scattering by convex obstacles. The problem is formulated as an integral equation. For the evaluation of the integral operators, a localized integration scheme is used. This, combined with a change of variables to resolve the problem of high slopes at the shadow boundaries, provides an efficient algorithm to solve the scattering problem for Helmholtz equation at high frequencies, with a computational cost that is independent of the frequency for a fixed accuracy.

Keywords: wave scattering; high frequency; localized integration; shadow points

Contents

Abstract ii

Table of Contents iii

Acknowledgements iv

1 Introduction 1
- 1.1 Motivation . . . 1
- 1.2 Problem . . . 2
- 1.3 Literature . . . 2
- 1.4 New Approach . . . 3

2 Theory 5
- 2.1 Boundary Integral Equation . . . 5
- 2.2 Integral Approximation . . . 6

3 Localization Technique 8
- 3.1 Partition of Unity . . . 8
- 3.2 Critical Points . . . 8
- 3.3 Exemplification . . . 9
- 3.4 Generalized Localization . . . 11

4 Numerical Method 12
- 4.1 Fourier Spectral Method . . . 12
- 4.2 Shadow Boundaries Problem . . . 13

5 Numerical Results 16

6 Conclusions 18

Appendix A 19

Bibliography 20

Acknowledgements

I want to give speacial thanks to Olof Runborg (Department of Numerical Analysis and Computer Science, the Royal Institute of Technology), who was my major research supervisor, for his invaluable guidance and insights. Without his tremendous support, my research would not be accomplished.

I am grateful to Alan Cline (Department of Computer Science, University of Texas at Austin) for serving as my thesis advisor and helping transform the research into a complete thesis. Moreover, he has been a dedicated teacher throughout my undergraduate education.

I also want to thank Björn Engquist (Department of Mathematics, University of Texas at Austin) and his wife, Elisabeth. They have provided enormous help in my going abroad to do research. In addition, Björn Engquist has reviewed and given useful comments on this research. He also has been a source of inspiration for my continued mathematical career.

Finally, I am thankful to Bruce Palka, Kit Belgum, Carrin Patman, and the Swedish Studies Excellence Endowment Scholarship committee, for supporting my research in Sweden.

Chapter 1

Introduction

1.1 Motivation

Numerical approximation of wave scattering is prevalent in many applications, including electromagnetic scattering, seismology, medical imaging, quantum physics, and photonics. For example, earthquakes are caused by the movement of seismic waves through the earth. Simulation of wave propagation is thus needed in order to study them.

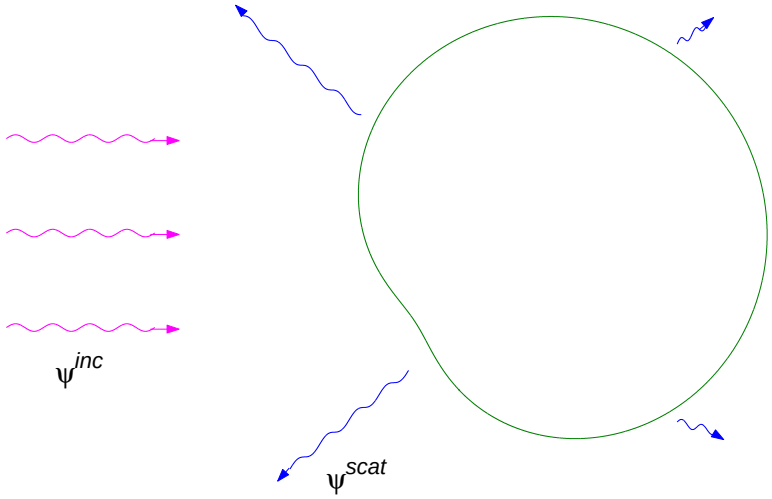

When the wave frequency is high, this is a multiscale problem: the small scale is given by the wavelength, and the large scale corresponds to the overall size of the computational domain [8]. This multiscale problem is important and a study of great interest. Seismic wave propagation, for instance, is a challenging elastic wave problem. High frequency approximations must be used when the relative wavelength is short. Medical ultrasonography, a modern technology used in medical imaging, uses high frequency sound waves of between 3.5 to 7.0 megahertz that are reflected by tissue to varying degrees to produce a 2D or 3D image. This is thus an inverse

scattering problem at high frequencies. The ultrasound imaging technology is often used to visualize the fetus in pregnant women. In computational electromagnetics radiation and scattering problems, eletromagnetics waves emited by radar devices often have a very short wavelength compared to the size of the scatterer, which can be an entire aircraft.

1.2 Problem

Consider the problem of computing the scattering of an incoming wave $\psi^{inc}(r) = e^{ik\alpha\cdot r}$, $|\alpha| = 1$, from a convex obstacle D. The scattered field ψ^{scat} satisfies the Helmholtz equation under Dirichlet boundary conditions:

$$\Delta\psi^{\text{scat}}(r) + k^2\psi^{\text{scat}}(r) = 0 \text{ in } \mathbb{R}^2 \setminus \bar{D} \tag{1.2.1}$$

$$\psi^{\text{scat}}(r) = -\psi^{\text{inc}}(r) \text{ on } \partial D, \tag{1.2.2}$$

and also satisfies the Sommerfeld radiation condition [6]

$$\lim_{r\to\infty} r\left[\frac{\partial\psi^{\text{scat}}}{\partial r} - ik\psi^{\text{scat}}\right] = 0,$$

i.e. ψ^{scat} vanishes as the distance approaches infinity.

When the wavelength is short, this is a difficult computational problem because of the highly oscillatory solution. In the direct discretization numerical simulation of (1.2.1), the accuracy of the solution is determined by the number of grid points or elements per wavelength. The computational cost to maintain constant accuracy grows at least linearly with the frequency, and for sufficiently high frequencies, direct numerical simulation is no longer feasible.

1.3 Literature

There are numerous numerical methods available for high frequency scattering problems. These methods can be classified into three main categories: direct methods, asymptotic methods, and hybrid methods.

Direct methods, such as Finite Element Methods (or FEM), are based on discretization of the computational domain into elements. If the boundary condition is given, the problem can be transformed into an integral equation on the boundary and only a mesh over the boundary is required. The accuracy of the solution is determined by the number of grid points per wavelength. Direct methods require a fixed number of discretization points per wavelength, and thus take at least $O(k)$ time to compute, where $k = \frac{2\pi}{\lambda}$ is the wave number.

On the other hand, most asymptotic techniques rely on Geometrical Optics (GO), which give the approximation of the phase and amplitude when the frequency tends to infinity. These unknowns typically vary much more slowly than the full solution. Hence, in principle, GO methods are easier to compute. Among the current state-of-the-art GO techniques are ray tracing methods [5, 13], wave-front methods: segment projection method [9] and level set methods [16], Hamilton-Jacobi methods for unique viscosity solutions [7] or multivalued solutions [10], and moment-based methods [2].

Hybrid methods, which combine both direct and asymptotic solvers, are also widely used [14]. The general idea is that direct methods are applied on parts which have similar scales to the wavelength and asymptotic techniques are applied elsewhere. For instance, hybrid methods are necessary if the scatterer is a large aircraft (large scale) with one or more antennas (small scale).

1.4 New Approach

Bruno, Geuzaine, Monro, and Reitich [3] have published a new convergent approach to solve high-frequency problems in $O(1)$ time for the case of convex scatterers. Like in direct methods, this approach also relies on discretization over the boundary of the obstacle. However, with the introduction of localized integration technique, only critical regions on the boundary are needed to be discretized, which makes the computation much easier. In [17], I have generalized and made the theory of their approach more rigorous. The purpose of this paper is to provide an implementation based on this theory and the numerical testing of the method. Such an explicit implementation has not been mentioned in [3]. I'll also compare my numerical results with the results of Bruno et al.

The convergent approach consists of the main elements below:

- Transform the Helmholtz Partial Differential Equation (PDE) to a Fredholm integral equation of the second kind, then replace the original unknown by a product of a slowly-oscillatory unknown function and a highly-oscillatory exponential with a known phase.

- Apply a localized integration scheme to integrate only around the critical points of the phase. The theoretical basis for this scheme is similar to the stationary phase method [1]. For high frequencies, the localization scheme tremendously reduces the number of integration points, while asymptotically maintaining the same accuracy. The asymptotic form of the Hankel function [6] combined with a piecewise analytic integration technique is used for integrating around the singular point of the kernel (see §3).

- Use a Fourier spectral method to solve the integral equation. A change of variables is used in order to compensate for the $O(k^{1/3})$ slopes at the shadow boundaries, thus to be able to represent the unknown function by a fixed number of Fourier coefficients within prescribed error tolerances (see §4).

The content of this paper is organized as following: in chapter 1, I will provide briefly the mathematical background that has been discussed in [17]. Chapter 2 will discuss the localization technique for fast numerical integration. In chapter 3, I will present the implementation of a Fourier spectral method to solve the integral equation. Chapter 4 and 5 will be numerical testing and conclusions, respectively. For the sake of simplicity, I present the method in two dimensions. In three dimensions, the idea of this approach can be applied in a similar manner.

Chapter 2

Theory

2.1 Boundary Integral Equation

The PDE in (1.2.1) under Dirichlet boundary conditions is transformed into a Fredholm integral equation of the second kind [3]:

$$\begin{aligned}\frac{1}{2}\mu(r) = \left(\frac{\partial\psi^{inc}(r)}{\partial\nu(r)} + i\gamma\psi^{inc}(r)\right) + \int_{\partial D}\frac{\partial G(r,r')}{\partial\nu(r')}\mu(r')ds(r') \\ + i\gamma\int_{\partial D} G(r,r')\mu(r')ds(r'),\end{aligned} \tag{2.1.1}$$

where

$$\mu(r) = \frac{\partial\psi(r)}{\partial\nu(r)}, \tag{2.1.2}$$

$$G(r,r') = \frac{i}{4}H_0^1(k|r-r'|), \tag{2.1.3}$$

and γ is an arbitrary regularizing constant in order to obtain the high numerical stability of the solution (see §4.1).

The function $\mu(r)$ in (2.1.1) is represented as:

$$\mu(r) = k\mu_{\text{slow}}(r)e^{ik\alpha\cdot r}. \tag{2.1.4}$$

As in Bruno et al., if D is a convex scatterer, μ_{slow} is a slowly oscillatory function of $r \in \partial D$. This is not true for a non-convex scatterer because of the possibility of multiple reflections. With the introduction of μ_{slow}, the original integral equation is equivalent to

$$\frac{1}{2}\mu_{\text{slow}}(r) - (\tilde{K}'\mu_{\text{slow}})(r) - i\gamma(\tilde{S}\mu_{\text{slow}})(r) = i\nu\cdot\alpha + i\frac{\gamma}{k}, \quad r \in \partial D, \tag{2.1.5}$$

where $\tilde{S}$ and $\tilde{K}'$ denote the integral operators

$$(\tilde{S}\mu_{\text{slow}})(r) = \int_{\partial D} G(r,r')e^{ik\alpha\cdot(r'-r)}\mu_{\text{slow}}(r')ds(r'), \tag{2.1.6}$$

$$(\tilde{K}'\mu_{\text{slow}})(r) = \int_{\partial D} \frac{\partial G(r,r')}{\partial \nu(r')}e^{ik\alpha\cdot(r'-r)}\mu_{\text{slow}}(r')ds(r'). \tag{2.1.7}$$

For $r' \neq r$, both kernels of the integrals in (2.1.6) and (2.1.7) behave asymptotically as

$$e^{ik[|r-r'|+\alpha\cdot(r'-r)]} =: e^{ik\phi}, \tag{2.1.8}$$

i.e. their dividing by $e^{ik\phi}$ are essentially non-oscillatory and independent of k.

In (2.1.5), the known kernels of the integral operators are the only highly oscillatory parts. I will show that within any prescribed error tolerance, μ_{slow} can be obtained after a fixed number of computational steps, independent of the frequency.

2.2 Integral Approximation

In this section, I provide two key lemmas for solving (2.1.5) described in §3 and §4.

Let $f_A(t) = S(t, cA, A) \times (1 - S(t, -A, -cA))$ and $f_\epsilon(t) = f_A(\frac{At}{\epsilon})$, where

$$S(t,t_0,t_1) = \begin{cases} 1 & \text{if } t \leq t_0, \\ \exp\left(\frac{2e^{-1/u}}{u-1}\right) & \text{if } t_0 < t < t_1,\ u = \frac{|t_1-t_0|}{t_1-t_0}, \\ 0 & \text{if } t \geq t_1. \end{cases}$$

(The function f_A, which was also used in Bruno et al., is thus smooth and compactly supported.)

Lemma 1[1]**.** *Suppose $\phi(t)$ is a real analytic function which has only one stationary point of order p at 0, i.e. $\phi^{(j)}(0) = 0$ $(\forall j = 1, 2, .., p)$ but $\phi^{(p+1)}(0) \neq 0$, and $h(t) \in C^\infty$ is a bounded function. Then:*

$$\left| \int_{-A}^{A} f_A(t)h(t)e^{ik\phi(t)}dt - \int_{-\epsilon}^{\epsilon} f_\epsilon(t)h(t)e^{ik\phi(t)}dt \right| = O\left((k\epsilon^{p+1})^{-n}\epsilon\right) \qquad \forall n \geq 1 \tag{2.2.1}$$

Corollary 1. *If we fix $\rho = k\epsilon^{p+1}$ $(\epsilon \sim k^{-\frac{1}{p+1}})$, $\int_{-\epsilon}^{\epsilon} f_\epsilon(t)h(t)e^{ik\phi(t)}dt$ is a good approximation of $\int_{-A}^{A} f_A(t)h(t)e^{ik\phi(t)}dt$ with a relative error of $O(\rho^{-n})$ $\forall n \geq 1$.*

This is a corollary of lemma 1 and the stationary point lemma [12]. The corollary implies that the integral $\int_{-A}^{A} f_A(t)h(t)e^{ik\phi(t)}dt$ can be approximated within a

[1] A generalization of this lemma will be discussed in §3.4

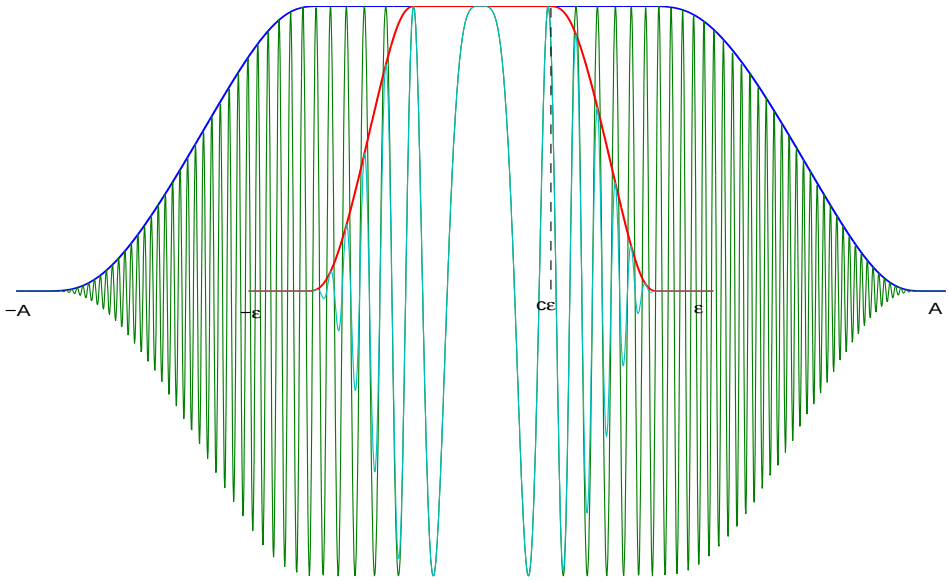

Figure 2.1: Upper-envelopes $f_A(t)$ and f_ϵ(t) and real part of the corresponding integrands.

prescribed error tolerance by integrating $\int_{-\epsilon}^{\epsilon} f_\epsilon(t)h(t)e^{ik\phi(t)}dt$ with a fixed number of discretization points, where $\epsilon \sim k^{-\frac{1}{p+1}}$ [17].

Lemma 2. *Suppose $\phi(t)$ is a real analytic function which has no stationary point on $[-A, A]$, and $h(t) \in C^\infty$ is a bounded function. Then:*

$$\left| \int_{-\epsilon}^{\epsilon} f_\epsilon(t)h(t)e^{ik\phi(t)} \right| = O\left((k\epsilon)^{-n}\epsilon\right) \qquad \forall n \geq 1 \text{ and } \forall \epsilon \leq A. \tag{2.2.2}$$

Corollary 2. *Suppose $\phi(t)$ is a real analytic function which has no stationary point on $[-A, A]$, and $h(t) \in C^\infty$ is a bounded function. Then:*

$$\left| \int_{-A}^{A} f_A(t)h(t)e^{ik\phi(t)} \right| = O\left(k^{-n}\right) \qquad \forall n \geq 1. \tag{2.2.3}$$

Chapter 3

Localization Technique

In this chapter, suppose that we want to compute the integral

$$\int_0^{2\pi} K(\theta_0,\theta)d\theta = \int_0^{2\pi} h(\theta_0,\theta)H_0^1(k|r-r_0|)e^{ik\alpha\cdot(r-r_0)}d\theta,$$

where $r = r(\theta)$ and $r_0 = r(\theta_0)$. Note that the Hankel function $H_0^1(x)$ is singular at $x = 0$ and asymptotically proportional to $\frac{e^{ix}}{\sqrt{x}}$ for $|x|$ large, hence $K \approx |K|e^{ik\phi}$ with the phase ϕ as in (2.1.8).

3.1 Partition of Unity

By partition of unity, 1 can be represented as a sum of upper-envelopes $f_A(\theta)$ centered at the critical points of $K(\theta_0,\theta)$ and their smooth cutoff complement, as illustrated in figure 3.2. Thus:

$$\int_0^{2\pi} K(\theta_0,\theta)d\theta = \sum \int_0^{2\pi} f_{A_j}(\theta)K(\theta_0,\theta)d\theta + \int_0^{2\pi} f_{\text{complement}}(\theta)K(\theta_0,\theta)d\theta.$$

As a result of Corollary 2, $\int_0^{2\pi} f_{\text{complement}}(\theta)K(\theta_0,\theta)d\theta$ is ignorable for k large enough. Following Corollary 1, the integrals $\int_0^{2\pi} f_{A_j}(\theta)K(\theta_0,\theta)d\theta$ can be localized so that only a fixed number of integration points is needed to obtain any prescribed error tolerance. The next section will explain what the critical points are.

3.2 Critical Points

The critical points of $K(\theta_0,\theta)$ are:

1. The target point $\theta = \theta_0$, where the kernel $K(\theta_0,\theta)$ is singular. This target point is covered by a region U_t of radius proportional to the wavelength λ ($p = 0$). Integrating around this singular point requires special consideration

since the kernel converges to ∞. Following Colton & Kress (1998) [6], we have:

$$H_0^1(k|x|) = \frac{2i}{\pi}\ln\frac{1}{|x|} + \frac{2i}{\pi}\ln\frac{1}{k} + C + O\left(|x|^2\ln\frac{1}{|x|}\right) \tag{3.2.1}$$

for $|x| \to 0$, where C is a constant. The function $L(\theta_0, \theta)$, defined as

$$L(\theta_0,\theta) = \frac{K(\theta_0,\theta)}{\frac{2i}{\pi}\ln\frac{1}{|\theta-\theta_0|} + \frac{2i}{\pi}\ln\frac{1}{k} + C},$$

is thus a bounded function. Piecewise linear approximation of $L(\theta_0, \theta)$ is used to compute the integral

$$\begin{aligned}
&\int_{\theta_0-\epsilon}^{\theta_0+\epsilon} K(\theta_0,\theta)d\theta \\
=&\frac{2i}{\pi}\int_{\theta_0-\epsilon}^{\theta_0+\epsilon}\ln\frac{1}{|\theta-\theta_0|}L(\theta_0,\theta)d\theta + C\int_{\theta_0-\epsilon}^{\theta_0+\epsilon}L(\theta_0,\theta)d\theta \\
\approx&\frac{2i}{\pi\Delta\theta}\sum_{j=-N/2}^{N/2-1}\int_{\theta_j}^{\theta_{j+1}}\ln\frac{1}{|\theta-\theta_0|}\left\{L(\theta_0,\theta_j)(\theta-\theta_{j+1}) + L(\theta_0,\theta_{j+1})(\theta-\theta_j)\right\}d\theta \\
&+ C\int_{\theta_0-\epsilon}^{\theta_0+\epsilon}L(\theta_0,\theta)d\theta
\end{aligned}$$

where $\Delta\theta = \frac{2\epsilon}{N}$ and $\theta_j = \theta_0 + j\Delta\theta$ for $j \neq 0$. The integrals in the sum can be evaluated exactly and $\int_{\theta_0-\epsilon}^{\theta_0+\epsilon} L(\theta_0,\theta)d\theta$ is approximated by the standard Trapezoidal rule.

2. The stationary points of the phase $\phi(\theta_0, \theta) = |r - r_0| + \alpha \cdot (r - r_0)$, at which ϕ has a vanishing gradient. Each stationary point is covered by a region U_s of radius proportional to $\sqrt{\lambda}$ ($p = 1$) or $\sqrt[3]{\lambda}$ ($p = 2$ at the shadow boundaries, where $\nu \cdot \alpha = 0$). The evaluation of stationary points for circular scatterers, as an example, is described in appendix A.

3.3 Exemplification

Let me exemplify the integration schemes above by computing the following integral on a circle of unit radius, centered at the origin:

$$I(\theta_0) = \int_0^{2\pi}\cos(\theta)H_0^1(k|r-r_0|)e^{ik\alpha\cdot(r-r_0)}d\theta, \tag{3.3.1}$$

with $r = r(\theta) = (\cos\theta, \sin\theta)$, $r_0 = r(\frac{\pi}{8})$, and $\alpha = (1, 0)$. Table 3.1 shows the fixed accuracy of the localized integrator using a fixed number of discretization points for all values of k.

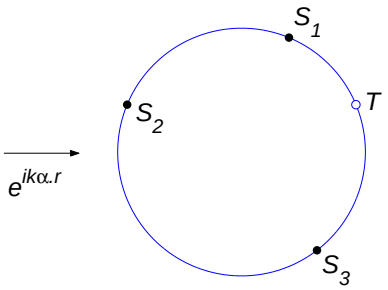

Figure 3.1: Circular scatterer under a plane incoming wave: target point T ($\theta_0 = \pi/8$) and stationary points S_1, S_2, S_3.

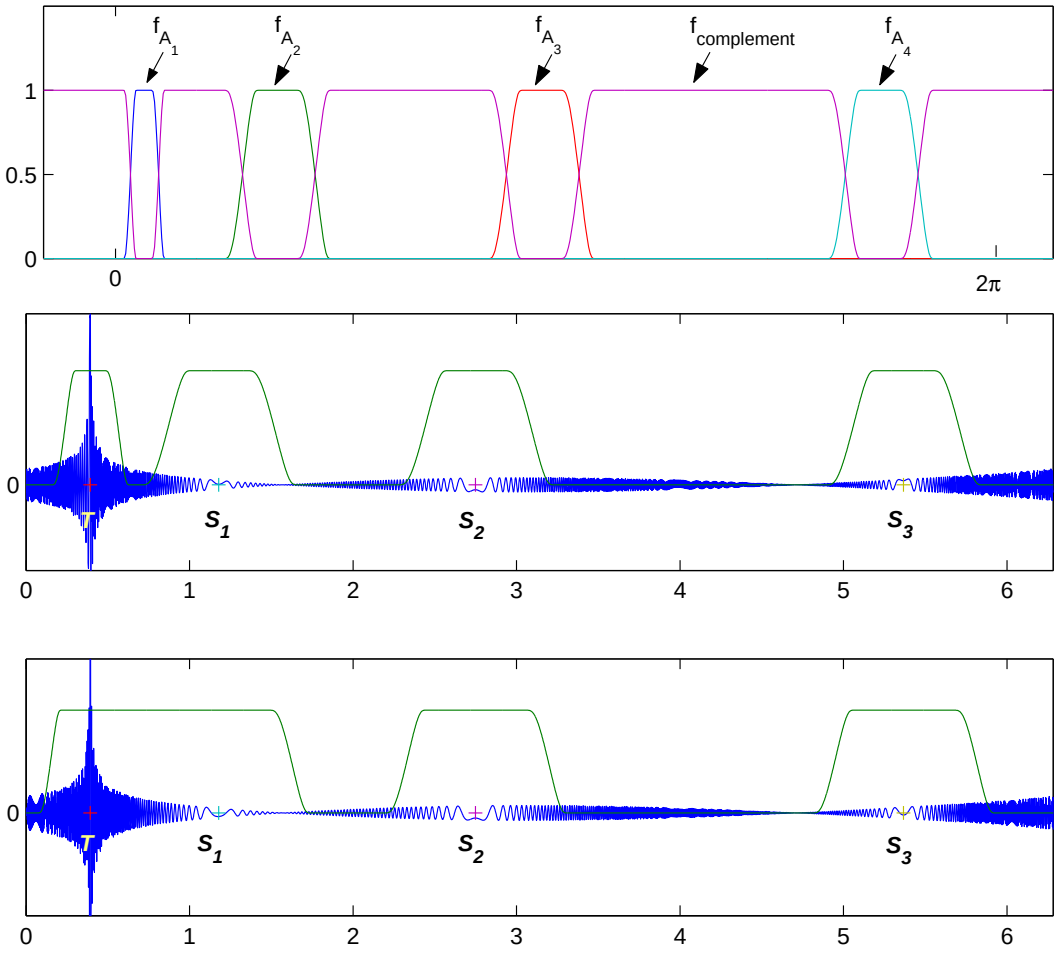

Figure 3.2: Covering for $\theta_0 = \pi/8$. Top: partition of unity. Middle: with $k = 4000$, no merging is needed. Bottom: with $k = 1500$, the smooth cutoff around the target point was merged with the one around the stationary point S_1. The quantity displayed in both graphs is the real part of the integrand in (3.3.1).

k	$\epsilon_t = \frac{500}{k}$	Relative error
500	1.0	1.06e-5
1000	0.5	8.58e-6
2000	0.25	3.06e-5
4000	0.125	6.47e-5
8000	0.0625	1.31e-5
16000	0.03125	2.14e-5
32000	0.015625	4.92e-6

Table 3.1: Error on $I(\theta_0 = \frac{\pi}{8})$ using 2000 discretization points (note: $\epsilon_s = \sqrt{\epsilon_t}$).

Note that, in Corollary 2, a certain width of the integrated region is required. Thus, a merger is needed in the implementation if the distance between any two integrated regions is below a threshold, which is proportional to $\frac{1}{k}$ as a result of Lemma 2. The covering around critical points and the merger are demonstrated in figure 3.2.

3.4 Generalized Localization

A critical point relatively close to the shadow points, with respect to the frequency (In practice, we do not solve the problem for $k = \infty$.), might cause difficulties, since the function $\phi(\theta_0, \theta)$ behaves as a cubic polynomial in the neighborhood of that point. This critical point therefore needs a wider covering.

Lemma 1* [17]. *Suppose $\phi(t)$ and $h(t)$ are as in Lemma 1, then:*

$$\left| \int_{-A}^{A} f_A(t) h(t) e^{ik\phi(t)} dt - \int_{-\epsilon}^{\epsilon} f_\epsilon(t) h(t) e^{ik\phi(t)} dt \right| = O\left(\left| k\epsilon\phi'(\epsilon) \right|^{-n} \epsilon \right) \quad \forall n \geq 1. \tag{3.4.1}$$

With this generalized lemma, we instead cover each critical point by a region of radius ϵ such that $|k\epsilon\phi'(\epsilon)| = \rho$, where ρ is the error parameter. The root finding can be done in constant time by means of Newton's method. Lemma 1* captures the behavior of the phase at an arbitrary point and the accuracy of the localized integration around that point.

Chapter 4

Numerical Method

With the integration techniques analyzed above, we now can go through the method of solving the integral equation (2.1.5).

4.1 Fourier Spectral Method

On the boundary, the function μ_{slow} is slowly oscillatory, smooth, and periodic. It can thus be well approximated by a finite Fourier sum:

$$\mu_{\text{slow}}\left(r(\theta)\right) \approx \sum_{n=-M}^{M} a_n e^{in\theta}.$$

Then:

$$\begin{aligned}
&\frac{1}{2}\mu_{\text{slow}}(r) - \int_0^{2\pi} K(\theta,\theta')\mu_{\text{slow}}(r')d\theta' = g(\theta) \\
\Rightarrow &\frac{1}{2}\sum_{n=-M}^{M} a_n e^{in\theta} - \sum_{n=-M}^{M} a_n \int_0^{2\pi} e^{in\theta'} K(\theta,\theta')d\theta' \approx g(\theta) \\
\Leftrightarrow &\sum_{n=-M}^{M} \left\{\frac{1}{2}e^{in\theta} - \int_0^{2\pi} e^{in\theta'} K(\theta,\theta')d\theta'\right\} a_n \approx g(\theta),
\end{aligned}$$

where $K(\theta,\theta') = \left\{G(r,r') + i\gamma\frac{\partial G(r,r')}{\partial\nu(r')}\right\} e^{ik\alpha\cdot(r'-r)}$ and $g(\theta) = i\nu\cdot\alpha + i\frac{\gamma}{k}$. Using $2M+1$ discretization points $\theta_m = 2\pi m/(2M+1)$, $v = [a_{-M}, a_{1-M}, ..., a_M]^T$ is obtained by solving the system of linear equations $Av = B$, where:

$$A[m,n] = \frac{1}{2}e^{in\theta_m} - \int_0^{2\pi} e^{in\theta'} K(\theta_m,\theta')d\theta', \tag{4.1.1}$$

$$B[m] = g(\theta_m). \tag{4.1.2}$$

The regularizing constant γ introduced in (2.1.1) is chosen appropriately to

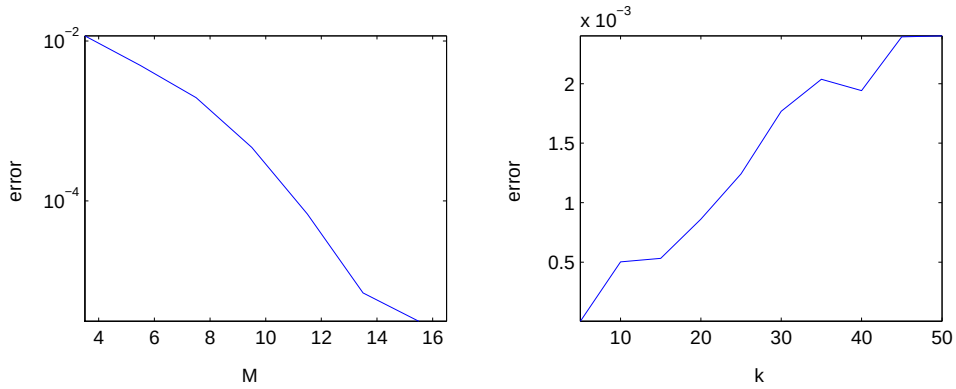

Figure 4.1: Errors of μ_{slow} with $\alpha = (1, 0)$. Left: with fixed $k = 5$ and various numbers of Fourier modes. Right: with $M = 15$ and various k's. A direct integration method was used: Simpson's rule with $20k$ discretization points over the region $[0, 2\pi]$.

make the matrix A well-conditioned. Following Bruno & Kunyansky (2001a) [4], I use $\gamma = 2R/\lambda = 2Rk$ ($2R$ is the diameter of the scatterer), which yields a low condition number of A. If $A[m, n]$ is computed by using the localized integrator, the computational time for solving (2.1.5) would be $O\left(M^2\right)$.

Figure 4.1 shows that the error decreases exponentially with respect to the number of Fourier coefficients. It also shows that with a fixed number of Fourier coefficients, the error increases unboundedly as k gets larger, due to the $O(k^{1/3})$ gradient of μ_{slow} at the shadow boundaries. Like in Bruno et al., I used L^2 erros to evaluate the accuracy of the numerical solution. Errors, computed by comparison with an exact solution for the integral equation, are defined as

$$\frac{\left\{\int_{\partial D} \left|\mu_{\text{slow}}(r) - \mu_{\text{slow}}^{\text{exact}}(r)\right|^2 ds(r)\right\}^{1/2}}{\left\{\int_{\partial D} \left|\mu_{\text{slow}}^{\text{exact}}(r)\right|^2 ds(r)\right\}^{1/2}}. \tag{4.1.3}$$

The next part will show how to achieve the fixed accuracy of μ_{slow} using a fixed number of Fourier coefficients.

4.2 Shadow Boundaries Problem

The number of Fourier modes needed to represent μ_{slow} with the same accuracy increases when k gets larger (see figure 4.1). This is explained by the steep slope, which is linear to $k^{1/3}$ [15, 3], at the shadow boundaries. In order to represent μ_{slow} within a prescribed error tolerance by a fixed number of coefficients, a change of

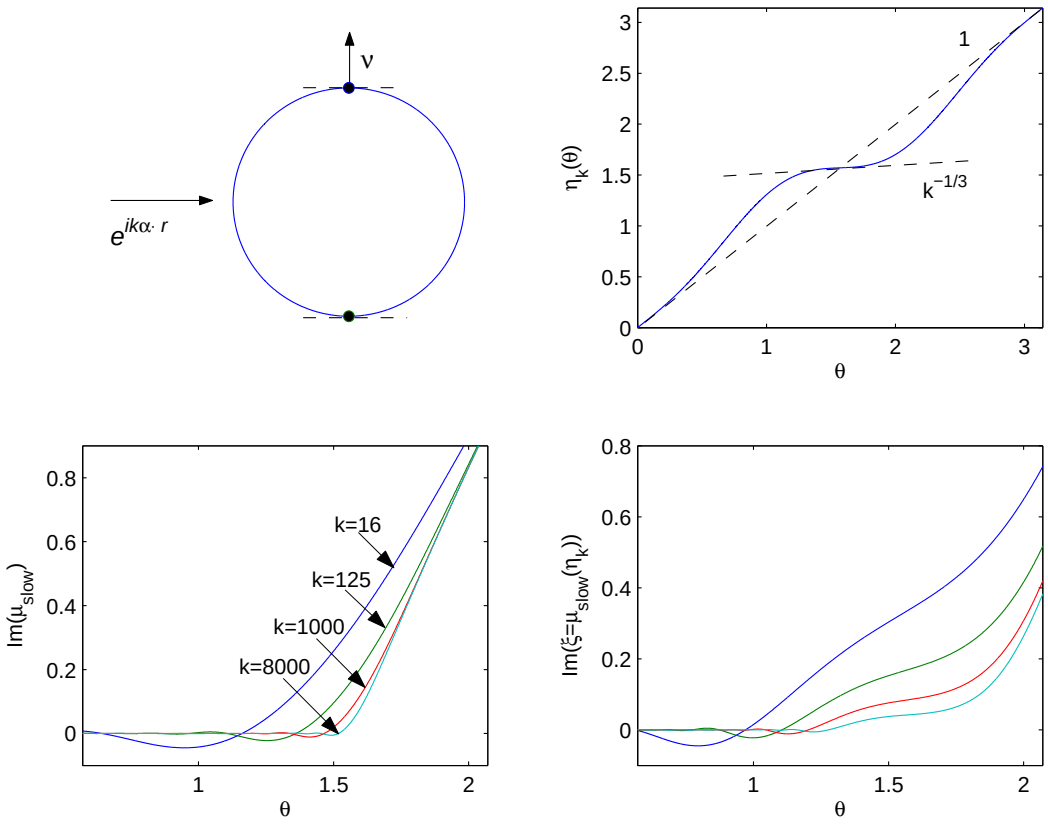

Figure 4.2: Top left: shadow boundaries for the circular scatterer. Top right: the change of variables function has slope of $k^{-1/3}$ at $\frac{\pi}{2}$. Bottom left: the gradient of μ_{slow} at $\frac{\pi}{2}$ gets steeper when k increases. Bottom right: the gradient of ξ is bounded with respect to k.

variables in μ_{slow} is applied [3]:

$$\xi(\theta) = \mu_{\text{slow}}(\eta_k(\theta)). \tag{4.2.1}$$

I choose $\eta_k(\theta) = \theta + \frac{1-k^{-1/3}}{4}\sin(2\theta) + \frac{k^{-1/3}-1}{8}\sin(4\theta)$ as the change of variables function. Figure 4.2 shows the behavior of η_k and the effect of this change of variables in $\mu_{\text{slow}}(\theta)$.

Since the slopes of $\xi(\theta)$ at the shadow boundaries are bounded, the function μ_{slow} can be represented as

$$\mu_{\text{slow}}(\theta) = \xi(\eta_k^{-1}(\theta)) = \sum_{n=-M}^{M} b_n e^{in\eta_k^{-1}(\theta)} \tag{4.2.2}$$

with a fixed accuracy and by a fixed M. Using a similar formulation as described in the previous section, we can find $v = [b_{-M}, b_{1-M}, ..., b_M]^T$, consequently compute ξ and μ_{slow}, by solving the system of linear equations $Av = B$. Here, I show two

M \ k	10	20	30	40	50
10	15	16.1	16.5	16.7	17.7
20	107	108.1	570	288	444.5
30	4e3	696	484	1.4e3	878
40	1.6e5	2.2e4	491	1e3	2e4

Table 4.1: The matrix A obtained in (4.2.3) has high condition numbers with different numbers of Fourier modes and different frequencies. The integral operators are computed using Simpson's rule with $20k$ discretization points.

M \ k	10	20	30	40	50
10	5.9	7.5	6.2	6.0	5.0
20	7.2	8.4	8.0	9.3	8.6
30	7.5	9.2	10.5	10.3	9.7
40	7.7	9.7	10.6	11.5	12.0

Table 4.2: The condition number of A is stably small when sampling $\eta_k^{-1}(\theta)$ uniformly.

different collocation schemes to obtain A and B with the change of variables:

1. By sampling $\theta_m = \theta$ in $\mu_{\text{slow}}(\theta)$ uniformly, we get:

$$A[m,n] = \frac{1}{2}e^{in\eta_k^{-1}(\theta_m)} - \int_0^{2\pi} e^{in\eta_k^{-1}(\theta')}K(\theta_m,\theta')d\theta' \tag{4.2.3}$$

   and B is as in (4.1.2). The scaling factor $\gamma = 2Rk$, however, no longer gives rise to the low condition number of A as shown in table 4.1, and thus does not guarantee the stability of the solution since the error might be magnified by a large number. A more appropriate choosing of γ is required for this scheme.

2. By sampling $\theta_m = \eta_k^{-1}(\theta)$ uniformly, we get:

$$A[m,n] = \frac{1}{2}e^{in\theta_m} - \int_0^{2\pi} e^{in\eta_k^{-1}(\theta')}K(\eta_k(\theta_m),\theta')d\theta', \tag{4.2.4}$$

$$B[m] = g(\eta_k(\theta_m)). \tag{4.2.5}$$

   Table 4.2 shows that using this scheme, the constant $\gamma = 2Rk$ guarantees a low condition number of A.

With this change of variables at the shadow boundaries, we can thus solve the integral equation (2.1.5) in constant time.

Chapter 5

Numerical Results

In figure 5.1, the errors of the solution are bounded when applying the change of variables with a fixed number of Fourier modes. The reference solutions are computed by using the spectral method described in §4.1 with $8\sqrt{k}$ Fourier modes. The integral operators of both the approximated and reference solutions are evaluated by using brute force Simpson's rule with $20k$ discretization points.

The results in table 5.1 demonstrate the bounded errors (less than 7×10^{-3}) of the solutions with various frequencies using the convergent method combined with changing of variables. For the parameters in the second column, 800 discretization points are needed for each localized integration. It takes roughly 13 minutes to compute the solution for every frequency when running this convergent method in Matlab on a Pentium IV 2.4GHz PC. Since the size of the matrix A is fixed and its elements are computed independently, this method can efficiently utilize parallel computing.

In the rightmost column, the parameters are changed ($|k\epsilon\phi'(\epsilon)| = 1000$, 4000 discretization points for each localized interval, and 150 Fourier modes to represent

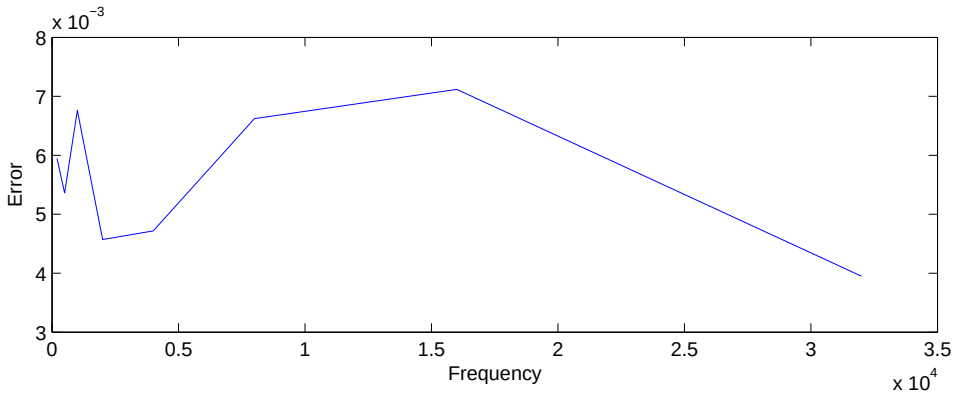

Figure 5.1: Errors of the solution with the change of variables (40 Fourier modes used).

Frequency	Errors of μ_{slow}	
	$\lvert k\epsilon\phi'(\epsilon)\rvert = 400$, 60 unknowns	$\lvert k\epsilon\phi'(\epsilon)\rvert = 1000$, 150 unknowns
1000	6.8e-3	7.1e-5
2000	4.4e-3	5.6e-6
4000	4.8e-3	4.5e-6
8000	6.4e-3	6.7e-6
16000	5.9e-3	5.7e-6
32000	3.2e-3	8.5e-6

Table 5.1: Accuracy of the convergent method combined with the change of variables. Errors are evaluated as in (4.1.3).

Frequency	Error	CPU Time
1	1.0e-12	$<$ 1s
10	3.0e-11	5s
100	1.5e-5	11s
1000	3.1e-5	2m30s
10000	8.4e-5	3m12s
100000	8.8e-5	3m43s

Table 5.2: Numerical results in Bruno et al.

the solution) to obtain a higher accuracy. The computational time of the solution for each frequency is about 3 hours. To achieve the same accuracy for $k = 1000000$, it would take at least 7 years to compute using the brute force method.

In their paper, Bruno et al. also provided their numerical results. These results, as shown in table 5.2 are somewhat inconsistent. For the frequencies less than 1000 and the presecribed tolerance of 10^{-4}, the localized integration scheme isn't more efficient than the direct method since the localized regions are too wide. This might explains the low running time for the first three frequencies in their testing. Thus, their high frequency solver was actually tested only three high frequencies. Even for these frequencies, there is still a slight increasing in the errors. This might be simply due the small sampling or it might also be due to the lack of a more generalized localization, i.e. Lemma 1*. Nevertheless, my numerical results have verified that by applying their convergent approach, a fixed-time algorithm for the high frequency scattering problems can be achieved.

Chapter 6

Conclusions

As a result of the boundary integral equation (2.1.1), the scattered field $\psi^{\text{scat}}(r)$ ($r \in \mathbb{R}^2 \setminus D$) can be obtained by evaluating the integral

$$\int_{\partial D} G(r, r') e^{ik\alpha \cdot r'} \mu_{\text{slow}}(r') ds(r').$$

This integral, whose kernel behaves asymptotically as $e^{ik[|r-r'|+\alpha \cdot r']}$, can be computed in constant time using the localized integration technique.

I have presented the implementation and numerical testing of a fixed-time numerical method for solving high frequency wave propagation problems for convex scatterers. This result can be generalized for non-convex scatterers using ray-tracing techniques, in which the representation in (2.1.4) is extended to:

$$\mu(r) = \sum_{j \geq 0} \mu^j_{\text{slow}} e^{ik\varphi^j(r)}, \tag{6.0.1}$$

where $\mu^j_{\text{slow}}(r)$ ($j \geq 1$) vanish on the convex part of the scatterer and $\varphi^j(r)$ ($j \geq 1$) are the phases of the new incoming waves due to reflections. With this extended formulation, the convergent method can be completed in a similar fashion [11].

Since the size of the matrix A in (4.2.4) is fixed and its elements can be computed independently, this method can effectively utilizes the power of parallel computing.

Appendix A: Evaluation of stationary points for circular scatterers

The stationary points correspond to the solutions of $\phi'(r_0, r) = 0$.

$$
\begin{aligned}
&\phi'(r_0, r) = (|r - r_0| + \alpha \cdot (r - r_0))' = 0 \\
\Leftrightarrow &\left(R\sqrt{\{\cos(\theta) - \cos(\theta_0)\}^2 + \{\sin(\theta) - \sin(\theta_0)\}^2} + R\cos(\theta - \alpha) - R\cos(\theta_0 - \alpha) \right)' = 0 \\
\Leftrightarrow &\left(\sqrt{2 - 2\left\{\cos(\theta)\cos(\theta_0) + \sin(\theta)\sin(\theta_0)\right\}} + \cos(\theta - \alpha) - \cos(\theta_0 - \alpha) \right)' = 0 \\
\Leftrightarrow &\left(\sqrt{2 - 2\cos(\theta - \theta_0)} \right)' + (\cos(\theta - \alpha))' = 0 \\
\Leftrightarrow &\left(\sqrt{4\sin^2\left(\frac{\theta - \theta_0}{2}\right)} \right)' - \sin(\theta - \alpha) = 0 \\
\Leftrightarrow &2\left|\sin\left(\frac{\theta - \theta_0}{2}\right)\right|' - \sin(\theta - \alpha) = 0 \\
\Leftrightarrow &\cos\left(\frac{\theta - \theta_0}{2}\right) - \sin(\theta - \alpha) = 0 \text{ (with } 0 \leq \theta - \theta_0 < 2\pi) \\
\Leftrightarrow &\frac{\theta - \theta_0}{2} = \frac{\pi}{2} - \theta + \alpha + 2n\pi \text{ or } \frac{\theta - \theta_0}{2} = -\frac{\pi}{2} + \theta - \alpha - 2n\pi
\end{aligned}
$$

A closed form can be given:

$$\theta_0 \leq \theta = (4n+1)\pi + 2\alpha - \theta_0 < \theta_0 + 2\pi \text{ or } \theta_0 \leq \theta = \frac{(4n+1)\pi + 2\alpha + \theta_0}{3} < \theta_0 + 2\pi.$$

Extension: for a non circular scatterer, the stationary points can be obtained by numerically solving the following nonlinear equation [3]

$$\frac{r(\theta)\frac{dr}{d\theta}(\theta) - r(\theta_0)\frac{dr}{d\theta}(\theta)\cos(\theta - \theta_0) + r(\theta_0)r(\theta)\sin(\theta - \theta_0)}{\sqrt{r(\theta_0)^2 + r(\theta)^2 - 2r(\theta_0)r(\theta)\cos(\theta - \theta_0)}} + \frac{dr}{d\theta}\cos(\theta) - r(\theta)\sin(\theta) = 0$$

on the interval $[\theta_0, \theta_0 + 2\pi)$.

Bibliography

[1] N. Bleistein and R. A. Handelsman. *Asymptotic Expansions of Integrals*. Dover, 1986.

[2] Y. Brenier and L. Corrias. A kinetic formulation for multibranch entropy solutions of scalar conservation laws. *Ann. Inst. Henri Poincaré*, 15(2):169–190, 1998.

[3] O. P. Bruno, C. A. Geuzaine, J. H. Monro Jr., and F. Reitich. Prescribed error tolerances within fixed computational times for scattering problems of arbitrarily high frequency: the convex case. *Phil. Trans. R. Soc. Lond. A*, 362:629–645, 2004.

[4] O. P. Bruno and L. A. Kunyansky. High-order algorithm for the solution of surface scattering problems: Basic implementation, tests, and applications. *Journal of Computational Physics*, 169:80–110, 2001a.

[5] V. Cerveny, I. A. Molotkov, and I. Psencik. *Ray Methods in Seismology*. Univ. Karlova Press, 1977.

[6] D. L. Colton and R. Kress. *Inverse Acoustic and Electromagnetic Scattering Theory (Applied Mathematical Sciences)*. Springer, 1998.

[7] M. G. Crandall and P.-L. Lions. Viscosity solutions of hamilton-jacobi equations. *Trans. Amer. Math. Soc.*, 277(1):1–42, 1983.

[8] B. Engquist and O. Runborg. Computational high frequency wave propagation. *Acta Numerica*, 12:181–266, 2003.

[9] B. Engquist, O. Runborg, and A.-K. Tornberg. High frequency wave propagation by the segment projection method. *J. Comput. Phys.*, 178:373–390, 2002.

[10] E. Fatemi, B. Engquist, and S. J. Osher. Numerical solution of the high frequency asymptotic expansion for the scalar wave equation. *J. Comput. Phys.*, 120(1):145–155, 1995.

[11] C. A. Geuzaine, Member, IEEE, O. P. Bruno, and F. Reitich. On the $o(1)$ solution of multiple-scattering problems. *IEEE Transactions on Magnetics*, 41(5), 2005.

[12] L. V. Hörmander. *The analysis of linear partial differential operators. I-IV*. Springer-Verlag, Berlin, 1983–1985.

[13] R. T. Langan, I. Lerche, and R. T. Cutler. Tracing of rays through heterogeneous media: An accurate and efficient procedure. *Geophysics*, 50:1456–1465, 1985.

[14] L. N. Medgyesi-Mitschang and D.-S. Wang. Hybrid methods for analysis of complex scatterers. *P. IEEE*, 77(5):770–779, 1989.

[15] R. B. Melrose and M. E. Taylor. Near peak scattering and the corrected Kirchhoff approximation for a convex obstacle. *Adv. Math.*, 55:242–315, 1985.

[16] S. J. Osher and J. A. Sethian. Fronts propagating with curvature-dependent speed: Algorithms based on hamilton-jacobi formulations. *J. Comput. Phys.*, 79(1):12–49, 1988.

[17] K. D. Tran. High frequency wave propagation: a convergent approach, part i. 2005.